Chinese Chemical Letters 33 (2022) 4691–4694

Contents lists available at ScienceDirect

Chinese Chemical Letters

journal homepage: www.elsevier.com/locate/cclet

Promoting electrochemical reduction of CO_2 to ethanol by B/N-doped sp^3/sp^2 nanocarbon electrode

Yanming Liu[a,b,*], Haolei Yang[a], Xinfei Fan[c], Bing Shan[b], Thomas J. Meyer[b,*]

[a] Key Laboratory of Industrial Ecology and Environmental Engineering (Ministry of Education), School of Environmental Science and Technology, Dalian University of Technology, Dalian 116024, China
[b] Department of Chemistry, University of North Carolina at Chapel Hill, Chapel Hill, North Carolina 27599, United States
[c] College of Environmental Science and Engineering, Dalian Maritime University, Dalian 116026, China

ARTICLE INFO

Article history:
Received 6 August 2021
Revised 7 October 2021
Accepted 23 December 2021
Available online 27 December 2021

Keywords:
CO_2 reduction
Ethanol
B/N-doped sp^3/sp^2 hybridized nanocarbon
Electrocatalysis
multi-carbon product

ABSTRACT

Electrochemical reduction of CO_2 to value-added chemicals holds promise for carbon utilization and renewable electricity storage. However, selective CO_2 reduction to multi-carbon fuels remains a significant challenge. Here, we report that B/N-doped sp^3/sp^2 hybridized nanocarbon (BNHC), consisting of ultra-small nanoparticles with a sp^3 carbon core covered by a sp^2 carbon shell, is an efficient electrocatalyst for electrochemical reduction of CO_2 to ethanol at relatively low overpotentials. CO_2 reduction occurs with a Faradaic efficiency of 58.8%-69.1% for ethanol and acetate production at $-0.5 \sim -0.6$ V (*vs.* RHE), among which 51.6%-56.0% is for ethanol. The high selectivity for ethanol is due to the integrated effect of sp^3/sp^2 carbon and B/N doping. Both sp^3 carbon and B/N doping contribute to enhanced ethanol production with sp^2 carbon reducing the overpotential for CO_2 reduction to ethanol.

Electrochemical reduction of CO_2 provides an attractive route for the synthesis of value-added fuels and chemicals, which could close the anthropogenic carbon cycle and store renewable energy. Recent progress on electrocatalytic CO_2 reduction has led to the production of CO, formate, acetate, alcohols and hydrocarbons with CO and formate as the most common products [1–5]. An important goal in this area is CO_2 reduction to highly reduced liquid products including multi-carbon alcohols. Success would provide a basis for producing sustainable fuels with high energy densities at costs less than current market prices [6]. Therefore, it is of interest to explore efficient CO_2 reduction electrocatalysts in favor of multi-carbon alcohols production.

Known electrocatalysts for CO_2 reduction include metals [7,8], metal oxides [9], metal complexes [10], heteroatom doped carbon materials [11,12] and their hybrid materials [13], among which copper-based electrocatalysts and heteroatom-doped carbon are capable of reducing CO_2 to multi-carbon oxygenates and hydrocarbons [14,15]. For these electrocatalysts, structure modification [16,17], oxidation state engineering [18], introduction of dopants [11,19,20] and alloys [21] have been used to steer CO_2 reduction toward multi-carbon alcohols. Although notable progress has been made, challenges remain for improving efficiency and decreasing the overpotential for CO_2 reduction to multi-carbon alcohols.

Heteroatom-doped carbon materials are attractive electrocatalysts with catalytic behaviors comparable to metal-based catalysts while having better stability [11,22]. In previous studies, we showed that heteroatom-doped diamond can catalyze C–C coupling reactions [11,23]. However, results from the previous studies required high overpotentials, and the method for diamond preparation limited its large-scale synthesis, as well as structure and composition modifications for enhancing catalytic performance. The sp^3/sp^2 hybrid nanocarbon (HC) is a cost-effective catalyst that can be prepared in large scales and modified to tailor catalytic performance by simpler method [24]. It integrates the good physicochemical properties of both sp^3 and sp^2 carbon for electrocatalysis. With heteroatom-doped sp^3-carbon, HC attains good electroreduction activity with a high overpotential for hydrogen evolution reaction, and sp^2 carbon can enhance electron transfer for catalysis [25,26]. Downsizing particle size to ultra-small favors exposing edge sites, and B/N doping into HC can create catalytic sites where the electron-deficient B and electron-rich N play synergistic roles in CO_2 reduction reaction. The combination of the two could boost CO_2 reduction activity and probably convert CO_2 to more reduced products such as multi-carbon alcohols.

Here we describe the use of ultra-small B/N-doped sp^3/sp^2 hybridized carbon (BNHC) nanoparticles for electrochemical reduction of CO_2 to ethanol, and the role of B/N doping and sp^3/sp^2 hy-

* Corresponding authors.
E-mail addresses: liuyanm@dlut.edu.cn (Y. Liu), tjmeyer@unc.edu (T.J. Meyer).

https://doi.org/10.1016/j.cclet.2021.12.063
1001-8417/

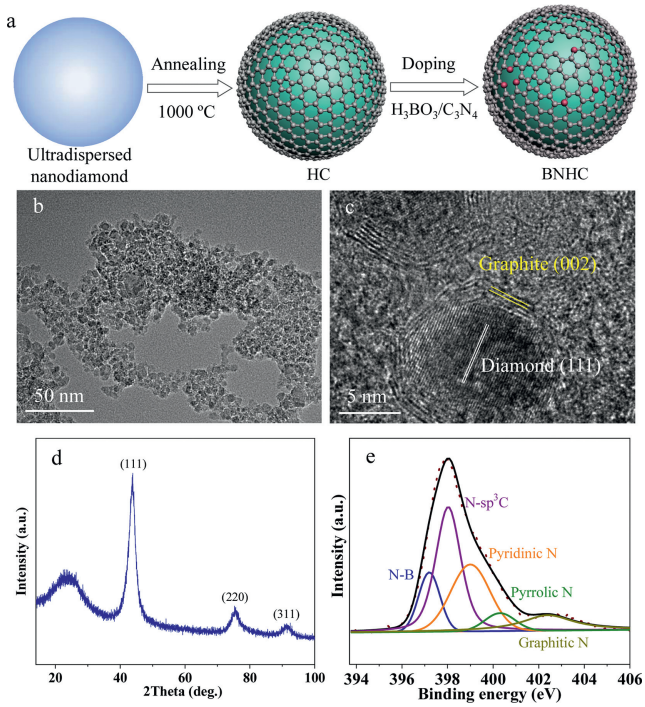

Fig. 1. (a) Schematic illustration of BNHC preparation, (b, c) TEM images, (d) XRD and (e) N 1s XPS spectra of BNHC.

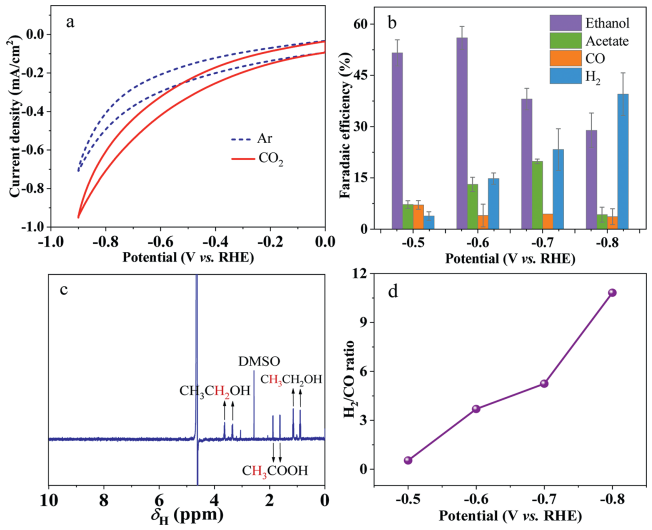

Fig. 2. (a) Cyclic voltammograms for BNHC in Ar or CO_2 saturated 0.1 mol/L $KHCO_3$ solutions (50 mV/s), (b) Faradaic efficiencies for ethanol, acetate, CO and H_2 production, (c) ^{1}H NMR spectrum of $^{13}CO_2$ reduction products (BNHC, −0.6 V *vs.* RHE), (d) mole ratios of H_2/CO from CO_2 reduction at BNHC.

brid carbon in CO_2 reduction. The combination of B/N doping and sp^3/sp^2 hybrid carbon provides a basis for CO_2 reduction to ethanol with high Faradaic efficiencies at relatively low overpotentials.

The BNHC electrocatalyst was synthesized by surface modification of ultra-dispersed nanodiamonds (Fig. 1a). In brief, the ultra-dispersed nanodiamonds were annealed at 1000 °C and oxidized by acid to obtain the sp^3/sp^2 hybridized nanocarbon (HC). B and N were doped into the HCs samples by calcining a mixture of HCs and H_3BO_3/C_3N_4 at 900 °C. Both transmission electron microscopy (TEM) and scanning electron microscopy (SEM) images showed that BNHC was composed of ultra-small nanoparticles (Figs. 1b and c and Fig. S1 in Supporting information). The BNHC nanoparticles had core-shell structures. The lattice spacing of the core was 0.204 nm, agreeing well with the (111) facet of diamond (sp^3-carbon). The interlayer spacing of the outer shell was 0.342 nm, consistent with the lattice distance for (002) facet of graphite (sp^2-carbon). The shell had a few layers of graphitic carbon. Energy dispersive X-ray spectroscopic maps showed B and N were distributed uniformly on BNHC (Fig. S2 in Supporting information).

The presence of sp^3 and sp^2 carbon in BNHC was confirmed by X-ray diffraction (XRD) pattern and Raman spectrum. In its XRD spectrum (Fig. 1d), diffraction peaks at 43.9°, 75.3° and 91.5° arise from cubic diamond with (111), (220) and (311) planes. The peak at 24.5° arises from the (002) plane of graphite. Peaks at 1343 cm^{-1} (D band) and 1570 cm^{-1} (G band) appeared in the Raman spectrum of BNHC (Fig. S3a in Supporting information). The D band is usually the characteristic peak for defects or sp^3 carbon, and the G band is from graphitic carbon. The intensity ratio of D and G bands (I_D/I_G) was 1.12, suggesting that BNHC has a relatively high proportion of sp^3 carbon and defects, both of which have been shown to contribute to electrocatalytic activity [25,27].

The results of XPS spectra showed that B and N were doped into HC (Fig. 1e and Fig. S3b in Supporting information). By deconvolution of the N 1s peak, N-B (397.2 eV), N-sp^3C (398.0 eV), pyridinic N (399.0 eV), pyrrolic N (400.3 eV) and graphitic N (402.4 eV) were found for BNHC, Among the N species, the content of N-sp^3C and pyridinic N was 67.8%. The high content of N-sp^3C and pyridinic N is favorable for electrocatalytic CO_2 reduction [11,28]. The B 1s spectrum (Fig. S3b) can be deconvoluted to four peaks, corresponding to BC_3 (190.0 eV), B-N (190.9 eV), BC_2O (191.6 eV) and BCO_2 (192.4 eV). The N content of BNHC was 5.2 at%, and its B content was 6.2 at% (Table S1 in Supporting information).

Electrochemical reduction of CO_2 on BNHC electrode was first explored by cyclic voltammetry. As shown in Fig. 2a, the current density in CO_2 saturated 0.1 mol/L $KHCO_3$ solution was increased compared to Ar saturated solution at potentials more negative than −0.2 V (*vs.* RHE), implying CO_2 reduction occurs on BNHC with a low onset potential. The product distribution following CO_2 electrolysis at BNHC electrodes was investigated at −0.5 V to −0.8 V (*vs.* RHE) in CO_2 saturated 0.1 mol/L $KHCO_3$ solution. The current densities were stable at the potentials used during steady-state CO_2 electrolysis (Fig. S4 in Supporting information). The liquid products were detected by ^{1}H NMR, and gas products were detected by gas chromatography. The analyses demonstrate the appearance of ethanol and acetate accompanied by a small amount of methanol and CO (Fig. S5 in Supporting information). To verify the origin of ethanol, acetate, methanol and CO, electrolysis was also carried out at BNHC electrode in Ar saturated 0.1 mol/L $KHCO_3$ solution at −0.6 V. The possible CO_2 reduction products including ethanol, acetate, methanol and CO were undetectable (Fig. S6 in Supporting information).

The Faradaic efficiencies in Fig. 2b showed that BNHC had a high selectivity for ethanol compared with acetate and CO (methanol with Faradaic efficiencies < 2.7% was negligible). For example, at −0.5 V and −0.6 V, the ethanol efficiency was 4.3–13.9 times higher than the efficiencies for acetate and CO. The ethanol efficiency was 51.6% at −0.5 V. It increased as the potential was lowered but declined after reaching a maximum value of 56.0% at −0.6 V. Given its performance, BNHC is one of the best electrodes reported for ethanol production (Table S2 in Supporting information). The Faradaic efficiencies for acetate increased from 7.2% to 19.8% when the potential was negatively shifted from −0.5 V to −0.7 V. The total Faradaic efficiencies for multi-carbon products, ethanol and acetate, were 57.9%–69.1% at −0.5 ~ −0.7 V. The commonly reported pathways for C2 production were surface adsorbed CO (*CO) dimerization [4,29]. When the potential decreased from

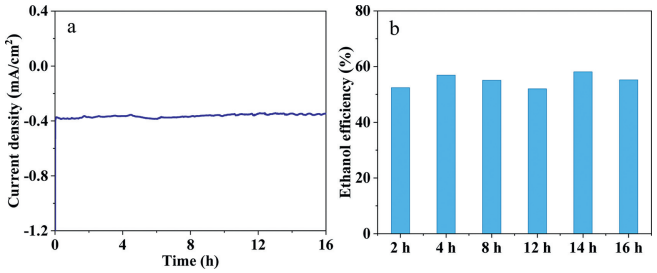

Fig. 3. (a) Current density and (b) Faradaic efficiencies for ethanol production during electrocatalytic CO_2 reduction for 16 h at −0.6 V (BNHC, 0.1 mol/L $KHCO_3$).

−0.5 V to −0.6 V, CO_2 reduction reaction could be enhanced to improve *CO coverage, which resulted in boosted *CO dimerization and thereby higher ethanol and acetate efficiencies. Since C2 production directly consumed *CO intermediates, CO efficiency decreased. However, competition from H_2 evolution reaction became increasingly fierce as the potential further decreased to or beyond −0.7 V, leading to decreased Faradaic efficiency for CO_2 reduction.

ICP-MS analysis and isotopic labeling experiment were performed to confirm that the detected products were from BNHC catalyzed CO_2 reduction. ICP-MS analysis revealed that its performance toward CO_2 reduction was not affected by trace metal impurities (details in Supporting information). $^{13}CO_2$ reduction was conducted on BNHC electrode at −0.6 V (*vs.* RHE). ^1H NMR spectrum of its products shows H-^{13}C signals for ethanol and acetate (Fig. 2c). Both split into two peaks from H-^{13}C spin coupling. The H-^{12}C signal for ethanol was of low intensity and was neglected in the analysis. The results are consistent with the generation of ethanol, acetate and CO from BNHC catalyzed CO_2 reduction.

In the gas phase, syngas with varying H_2/CO molar ratios from 0.5 to 10.8 was found for BNHC catalyzed CO_2 reduction (Fig. 2d). The H_2/CO ratio increased gradually as the potential was more negative. Syngas is an important feedstock for chemicals and fuels production. The potential-dependent H_2/CO ratio observed here can meet the demands imposed by downstream chemicals and fuels synthesis. Application of this electrochemical method for syngas production, with adjustable H_2/CO ratio, is straightforward and applicable for industrial process.

The stability of BNHC electrode toward long-term electrocatalytic CO_2 reduction was examined by CO_2 electrolysis over a period of 16 h at −0.6 V. As shown in Fig. 3a, its current density was stable during 16 h of CO_2 electrolysis after reaching the initial steady state current density. During the process of CO_2 reduction, the ethanol efficiency was probed every 2 h with results presented in Fig. 3b. The data demonstrated that ethanol efficiency was maintained at ~56.0% with BNHC electrode stable for at least 16 h. Energy dispersive X-ray spectroscopy showed a uniform distribution of B and N after CO_2 reduction (Fig. S7 in Supporting information). The contents of B and N were 6.3 at% and 4.6 at% after reaction, similar to 6.2 at% and 5.2 at% before reaction. (Table S1). By deconvolution of B and N 1s XPS peak (Fig. S8 in Supporting information), the B species remained the same while the content of pyridinic N declined 0.56 at% (Table S3 in Supporting information) after reaction. This phenomenon can be explained by that pyridinic N weakly binds with CO_2 in a similar way as in pyridine catalyzed homogenous CO_2 reduction, which generates pyridinium-CO_2 complex (pyridonic N) intermediate. The stable CO_2 reduction performance indicated the conversion between pyridinic N and pyridonic N may be reversible [30,31]. Diffraction peaks of graphite (002) plane and diamond (111), (220) and (311) plane still can be observed on its XRD spectrum (Fig. S9 in Supporting information).

To investigate the effect of B/N doping on CO_2 reduction products distribution, CO_2 reduction was conducted at the HC electrode. The HC electrode was prepared by the same method as BNHC electrode without doping, and its electrocatalytic performance for CO_2 reduction was compared with BNHC. XRD data showed that HC had (111), (220) and (311) planes of cubic diamond along with (002) plane of graphite (Fig. S10a in Supporting information), the same crystalline structure as BNHC. In the Raman spectrum of HC (Fig. S10b in Supporting information), both peaks related to sp^2 carbon (G band), sp^3 carbon and defects (D band) were observed. The intensity ratio of D band and G band was 0.99, smaller than 1.12 for BNHC, which can be attributed to the fact that B/N doping introduces defects into the BNHC structure.

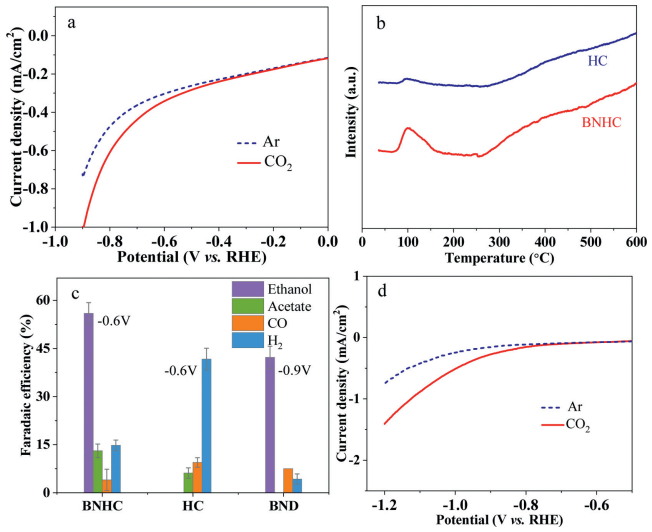

Fig. 4. (a) Linear sweep voltammograms for HC in Ar or CO_2 saturated 0.1 mol/L $KHCO_3$ solutions, (b) the temperature-programmed CO_2 desorption curves of BNHC and HC, (c) comparison of CO_2 reduction efficiencies with BNHC, HC and BND electrodes, (d) linear sweep voltammograms of BND in Ar or CO_2 saturated 0.1 mol/L $KHCO_3$ solution (scan rate of 50 mV/s).

Linear sweep voltammogram showed that HC was also active for electrochemical reduction of CO_2 (Fig. 4a). However, it showed more negative onset potential (~ −0.4 V) than BNHC. Its current density increasement, during Ar saturated solution switched to CO_2 saturated solution, was not as significant as that for BNHC, suggesting that BNHC was more active than HC toward electrocatalytic CO_2 reduction. The temperature-programmed desorption of CO_2 analysis (Fig. 4b) showed the appearance of CO_2 desorption peaks at 70–175 °C and 260–485 °C for BNHC. They can be attributed to physical adsorption or weak chemical adsorption of CO_2 and strong chemical adsorption of CO_2, respectively. However, HC exhibited much weaker CO_2 desorption peaks than BNHC, demonstrating that the CO_2 adsorption capability was enhanced after B/N doping.

The results of CO_2 electrolysis (−0.6 V) showed products for HC were acetate and CO along with large amount of hydrogen, and ethanol was undetectable under the applied conditions (Fig. 4c). The Faradaic efficiency for acetate production was 6.2%. Compared with BNHC, HC exhibited a significantly decreased Faradaic efficiency for multi-carbon products generation, which indicates B/N doping plays important roles for reducing CO_2 to multi-carbon products. Given that C1 products are commonly produced on heteroatom-doped graphitic carbon electrodes [22,28,32,33], the high efficiency for C2 production on BNHC could be mainly contributed from B/N-doped sp^3 carbon. The doped N and B worked in tandem to promote ethanol generation, where N doping facilitates H transfer and B doping stabilizes the intermediates for ethanol production [23].

The effect of sp^2 carbon shell on electrocatalytic CO_2 reduction was probed by comparing the CO_2 reduction performance of BNHC with B/N-doped diamond (BND, sp^3 carbon) with neglectable sp^2 carbon. BND was prepared by hot filament chemical vapor deposition [23] (unable to prepare BND by the similar method as BNHC). As shown by the SEM image in Fig. S11 (Supporting information), BND exhibited a nanoparticle morphology. It has an identical crystalline diamond structure (Fig. S12 in Supporting information) and similar B/N content (Table S1) as BNHC. Its onset potential for CO_2 reduction was about −0.7 V (Fig. 4d), much more negative than BNHC (−0.2 V). Herein, electrocatalytic CO_2 reduction was conducted at −0.9 V on BND electrode. Analysis of the products showed ethanol and CO were produced by BND catalyzed CO_2 reduction but acetate was undetectable. Fig. 4c showed the Faradaic efficiency for ethanol production on BND (−0.9 V) was lower than on BNHC (−0.6 V, comparison between BNHC-0.9 V and BND-0.9 V was shown in Fig. S13 in Supporting information). However, its efficiency for C2 products was much higher than HC. The data show that introduction of sp^2 carbon on BNHC can reduce the overpotential for CO_2 reduction and promote C2 production. It also confirms that both B/N doping and sp^3 carbon contribute to the high performance of BNHC in C2 production. To explore the effect of electrode surface area on ethanol production, partial current density for ethanol was normalized by electrochemically active surface area (EASA). Although the EASA of BNHC was higher than BND (Figs. S14a-c in Supporting information), BNHC showed higher normalized partial current density for ethanol than BND (Fig. S14d in Supporting information), revealing the higher intrinsic activity of BNHC for ethanol production.

In summary, metal-free B/N-doped sp^3/sp^2 nanocarbon electrode consisting of ultra-small core-shell nanoparticles is developed for selectively electrochemical reduction of CO_2 to ethanol. Contributed from the integrated effects of B/N doping, sp^3 and sp^2 carbon, the BNHC electrode is efficient for reduction of CO_2 to ethanol and acetate with high Faradaic efficiencies of 58.8%−69.1% at $-0.5 \sim -0.6$ V (*vs.* RHE), among which 51.6%−56.0% is for ethanol production. These results provide new insights for the design of efficient electrocatalysts to steer CO_2 reduction towards multi-carbon products with high selectivity.

Declaration of competing interest

The authors declare that they have no known competing financial interests or personal relationships that could have appeared to influence the work reported in this paper.

Acknowledgments

This work was supported by National Natural Science Foundation of China (Nos. 22076019 and 21707016), The Youth Talent Support Program of Liaoning Province (No. XLYC2007069) and U.S. Department of Energy (DOE), Office of Basic Energy Sciences under Award (No. DE-SC0015739).

Supplementary materials

Supplementary material associated with this article can be found, in the online version, at doi:10.1016/j.cclet.2021.12.063.

References

[1] H. Wang, Y.K. Tzeng, Y. Ji, et al., Nat. Nanotechnol. 15 (2020) 131–137.
[2] X. Yuan, L. Zhang, L. Li, et al., J. Am. Chem. Soc. 141 (2019) 4791–4794.
[3] Z.Z. Niu, F.Y. Gao, X.L. Zhang, et al., J. Am. Chem. Soc. 143 (2021) 8011–8021.
[4] C.T. Dinh, T. Burdyny, M.G. Kibria, et al., Science 360 (2018) 783–787.
[5] T. Möller, W. Ju, A. Bagger, et al., Energy Environ. Sci. 12 (2019) 640–647.
[6] O.S. Bushuyev, P. De Luna, C.T. Dinh, et al., Joule 2 (2018) 825–832.
[7] J.J. Lv, M. Jouny, W. Luc, et al., Adv. Mater. 30 (2018) e1803111.
[8] K. Jiang, S. Siahrostami, T. Zheng, et al., Energy Environ. Sci. 11 (2018) 893–903.
[9] H. Jung, S.Y. Lee, C.W. Lee, et al., J. Am. Chem. Soc. 141 (2019) 4624–4633.
[10] M.D. Sampson, C.P. Kubiak, J. Am. Chem. Soc. 138 (2016) 1386–1393.
[11] Y. Liu, S. Chen, X. Quan, H. Yu, J. Am. Chem. Soc. 137 (2015) 11631–11636.
[12] D. Luo, S. Liu, K. Nakata, A. Fujishima, Chin. Chem. Lett. 30 (2019) 509–512.
[13] J. Sun, W. Zheng, S. Lyu, et al., Chin. Chem. Lett. 31 (2020) 1415–1421.
[14] Y. Zheng, A. Vasileff, X. Zhou, et al., J. Am. Chem. Soc. 141 (2019) 7646–7659.
[15] R.M. Arán-Ais, F. Scholten, S. Kunze, R. Rizo, B.Roldan Cuenya, Nat. Energy 5 (2020) 317–325.
[16] Q. Zhang, D. Ren, S. Pan, et al., Adv. Funct. Mater. 31 (2021) 2103966.
[17] P.P. Yang, X.L. Zhang, F.Y. Gao, et al., J. Am. Chem. Soc. 142 (2020) 6400–6408.
[18] X. Yuan, S. Chen, D. Cheng, et al., Angew. Chem. Int. Ed. 60 (2021) 15344–15347.
[19] Y. Zhou, F. Che, M. Liu, et al., Nat. Chem. 10 (2018) 974–980.
[20] Y. Jiao, Y. Zheng, P. Chen, M. Jaroniec, S.Z. Qiao, J. Am. Chem. Soc. 139 (2017) 18093–18100.
[21] E.L. Clark, C. Hahn, T.F. Jaramillo, A.T. Bell, J. Am. Chem. Soc. 139 (2017) 15848–15857.
[22] J. Wu, T. Sharifi, Y. Gao, T. Zhang, P.M. Ajayan, Adv. Mater. 31 (2019) e1804257.
[23] Y. Liu, Y. Zhang, K. Cheng, et al., Angew. Chem. Int. Ed. 56 (2017) 15607–15611.
[24] Y. Lin, X. Sun, D.S. Su, G. Centi, S. Perathoner, Chem. Soc. Rev. 47 (2018) 8438–8473.
[25] N. Yang, S. Yu, J.V. Macpherson, et al., Chem. Soc. Rev. 48 (2019) 157–204.
[26] Y. Zhu, Y. Lin, B. Zhang, et al., ChemCatChem 7 (2015) 2840–2845.
[27] J. Wu, M. Liu, P.P. Sharma, et al., Nano Lett. 16 (2016) 466–470.
[28] F. Pan, B. Li, X. Xiang, G. Wang, Y. Li, ACS Catal. 9 (2019) 2124–2133.
[29] W. Luc, X. Fu, J. Shi, et al., Nat. Catal. 2 (2019) 423–430.
[30] B. Kumar, M. Asadi, D. Pisasale, et al., Nat. Commun. 4 (2013) 2819.
[31] E.B. Cole, P.S. Lakkaraju, D.M. Rampulla, et al., J. Am. Chem. Soc. 132 (2010) 11539–11551.
[32] H. Wang, J. Jia, P. Song, et al., Angew. Chem. Int. Ed. 56 (2017) 7847–7852.
[33] S. Zhang, P. Kang, S. Ubnoske, et al., J. Am. Chem. Soc. 136 (2014) 7845–7848.